Experimental Plasma Physics Branch
Plasma Physics Division

September 15, 1980

REPORT DOCUMENTATION PAGE	READ INSTRUCTIONS BEFORE COMPLETING FORM

1. REPORT NUMBER NRL Memorandum Report 4297	2. GOVT ACCESSION NO. AD-A089372	3. RECIPIENT'S CATALOG NUMBER NRL-MR-4-77

4. TITLE (and Subtitle) COMPUTER SIMULATION STUDIES OF THE TEARING MODE INSTABILITY IN A FIELD-REVERSED ION LAYER	5. TYPE OF REPORT & PERIOD COVERED Interim report on a continuing NRL problem.
	6. PERFORMING ORG. REPORT NUMBER

7. AUTHOR(s) S.J. Marsh*, A.T. Drobot** and C.A. Kapetanakos	8. CONTRACT OR GRANT NUMBER(s) RD1104

9. PERFORMING ORGANIZATION NAME AND ADDRESS Naval Research Laboratory Washington, D.C. 20375	10. PROGRAM ELEMENT, PROJECT, TASK AREA & WORK UNIT NUMBERS 61153N; RR0110941 67-0869-0-0

11. CONTROLLING OFFICE NAME AND ADDRESS Office of Naval Research Arlington, Virginia 22217	12. REPORT DATE Sep 80
	13. NUMBER OF PAGES 37

14. MONITORING AGENCY NAME & ADDRESS(if different from Controlling Office)	15. SECURITY CLASS. (of this report) UNCLASSIFIED
	15a. DECLASSIFICATION/DOWNGRADING SCHEDULE

16. DISTRIBUTION STATEMENT (of this Report)

Approved for public release; distribution unlimited.

17. DISTRIBUTION STATEMENT (of the abstract entered in Block 20, if different from Report)

19. KEY WORDS (Continue on reverse side if necessary and identify by block number)

Ion rings
Ion layers
Instabilities
Tearing mode

20. ABSTRACT (Continue on reverse side if necessary and identify by block number)

Results are reported on the computer simulation of a long, space charge neutral ion layer. The critical axial velocity spread required to stabilize the tearing mode is in agreement with the predictions of Uhm and Davidson. The growth rates of individual modes depend on the evolving profile of the distribution functions. For initially square velocity distribution profile, the code predicts growth rates that are slower by about a factor of two than

(Abstract continues)

DD FORM 1 JAN 73 1473 EDITION OF 1 NOV 65 IS OBSOLETE
S/N 0102-LF-014-6601

i

20.   (Abstract continued)

those of the linear theory. In addition, it has been demonstrated that when the Budker parameter of the layer ν exceeds 1/3, a conducting wall surrounding the layer may have a destabilizing influence on it.

CONTENTS

iii

COMPUTER SIMULATION STUDIES OF THE TEARING MODE INSTABILITY IN A FIELD-REVERSED ION LAYER

I.   INTRODUCTION

The advent of pulsed, high power ion sources[1] during
the last several years has stimulated renewed interest in
the formation of field-reversed configurations (FRC) with
ion rings or layers. Similarly, the availability of intense,
long duration neutral beams has focused attention on the
possibility of forming field-reversed configurations in an
ordinary magnetic mirror by either ion layers[2] or plasma
currents.[3] Presently, thermonuclear reactors based on such
field-reversed configurations look very attractive because
their anticipated high power density might lead to relative
low cost and modest size systems.[4]

The usefulness of ion ring or layer generated FRC rests
very heavily on their stability. As a result of the complexity
of the problem, no comprehensive treatment of the stability of
such states is presently available. However, all the results
obtained so far are very encouraging. Using the energy prin-
ciple Sudan and Rosenbluth[5] have shown with a hybrid model
that a field-reversed ion layer immersed in a background
plasma is stable against MHD kink modes when its aspect ratio
(= major radius/minor radius) is near unity. Lovelace[6] had
arrived earlier at a similar conclusion. Uhm and Davidson[7]
have treated the stability of a field-reversed layer for
frequencies near multiples of the mean rotational frequency

of the layer. They have found that these instabilities, which are of primary concern can be easily stabilized by introducing transverse temperature in the rotating ions of the layer. Finn and Sudan[8] have investigated the effect of particle resonances on low-frequency magnetohydrodynamic modes in a field reversed, long ion layer.

The tearing modes, i.e., low frequency instabilities that break up a very long layer into several rings have been studied by Marx[9] and recently by Uhm and Davidson.[10] Fowler[11] has found that finite length layers are stable to tearing modes as a consequence of axial kinetic pressure. Using a hybrid model, in which the ion layer is treated kinetically and the background plasma as a fluid, Uhm and Davidson extended the calculation of Fowler to infinitely long layers and have shown that when the axial velocity spread Δv exceeds a critical value Δv_{crit}, the layer does not break into rings, i.e., is stable to the tearing mode.

In this paper, we report results from the numerical simulation of an infinitely long, space-charge neutral ion layer. The numerical results give a Δv_{crit} that is in excellent agreement with the theory. However, the growth rates predicted by the theory are always greater by a factor of two than those found from the code. An interesting result of the simulation is that although close-fitted metal walls always improve the stability of an unstable layer, there

are conditions under which a conducting shell that is not very near the outer edge of the layer can have an adverse effect on the stability of the layer.

In Section II of this paper we give a brief description of the particle-in-cell code used for these studies. The initiation of the rigid rotor equilibrium with finite temperature is also described as are the basic diagnostics for determining the energy of the magnetic field spectrum. The linear theory for the onset of the tearing mode is reviewed in Section III. It is clear from the interpretation of the threshold condition that there exist regimes where the presence of a conducting wall can have a destabilizing influence on the tearing mode. In Section IV we present the results of the simulation which confirm the existence of the threshold condition as determined by the thermal spread in the parallel velocity V_z and the geometric position of the beam.

The effect of wall destabilization is also demonstrated as discussed in the conclusion presented in Section V.

II. DESCRIPTION OF THE CODE

    a)   Field Solver

The dynamics of reversed magnetic field ion layers are studied in a cylindrical, azimuthally symmetric (r,z) geometry using a 2D-3V particle simulation code.[12] The annular proton layers are space-charge neutralized by electrons which follow the radial and axial motion of ions thus cancelling

the ion current in these directions. The electrons, however, do not cancel the azimuthal ion current. Thus, Maxwell's equations reduce to

$$\nabla^2 A_\theta - \frac{A_\theta}{r^2} = - \mu_o J_\theta ,$$

where A_θ (r,z,t) is the magnetic vector potential, J_θ (r,z,t) is the self consistant ion current and μ_o is the permeability of free space.

For this azimuthally symmetric system B_z and B_r are obtained by differentiating A_θ. The canonical angular momentum $P_\theta = r(m_i V_\theta + qA_\theta)$ is a constant of the motion and is used to find V_θ of each ion.

The magnetic vector potential A_θ is solved on a two dimensional (r,z) grid (typically 32 x 32 but expandable to 32 x 128) by Fourier analysis in the axial direction and by Gaussian elimination in the radial direction. The system is periodic in z and is enclosed radially by a perfectly conducting wall. The standard five point difference operator is used to represent the differential operator ∇^2.

The equations of motion are solved in a leapfrog scheme.

$$V_{\theta_i}^{T+\frac{1}{2}} = \frac{P_{\theta_i}}{M_i r_i^{T+\frac{1}{2}}} - \frac{|e|}{M_i} A_{\theta_i}^{T+\frac{1}{2}}$$

$$V_{R_i}^{T+1} = V_{R_i}^{T} + \Delta T V_{\theta_i}^{T+\frac{1}{2}} \left(\frac{V_{\theta_i}^{T+\frac{1}{2}}}{r_i^{T+\frac{1}{2}}} + \frac{|e|}{M_i} B_{z_i}^{T+\frac{1}{2}} \right)$$

$$V_{z_i}^{T+1} = V_{z_i}^{T} - \Delta T \frac{|e|}{M_i} V_{\theta}^{T+\frac{1}{2}} B_{R_i}^{T+\frac{1}{2}}$$

$$r_i^{T+3/2} = r_i^{T+\frac{1}{2}} + \Delta T V_{R_i}^{T+1}$$

$$z_i^{T+3/2} = z_i^{T+\frac{1}{2}} + \Delta T V_{z_i}^{T+1} \quad ,$$

where ΔT is the unit timestep and T is the time. The fields B_{z_i}, B_{r_i} and vector potential A_{θ_i} are found at the particle positions by volume averaging the fields at the four nearest cells.

The field solver and particle pusher are not naturally time centered. The lack of centering can and does cause the solution of the field solver to become numerically unstable.

To obtain a numerically stable solution we rewrite the differential equation for A_θ as

$$\nabla^2 \left(\frac{A_{K+1}^{T+3/2} + A_K^{T+3/2}}{2} \right)$$

$$= J_K^{T+3/2} + \alpha \left(A_{K+1}^{T+3/2} - A_K^{T+3/2} \right) ,$$

where $A_{K+1}^{T+3/2} = A_\theta \left((T + 3/2)\Delta t \right)$ is the new solution, $A_0^{T+3/2} = A_\theta \left((T + 1/2)\Delta t \right)$ is the solution from the previous time step,

$$J_K^{T+3/2} = J_\theta \left((T+3/2)\Delta t \right) = ne \sum_{i\,=\,1} \left(\frac{P_{\theta_i}}{mr_i} - \frac{q}{m} A_{k,i} \right) ,$$

α is a suitably chosen constant

P_θ is the canonical angled momentum of the ith particle,

r_i is the radial position of ith particle,

$A_{k,i} = A_K^{T+3/2}$ evaluated at the position of the ith particle and K is the iteration number.

The equation can be written as

6

$$\nabla^2 A_{K+1} - 2\alpha A_{K+1}$$

$$= 2J_K - \nabla^2 A_K - 2\alpha A_K$$

$$= 2J_K - \left(\nabla^2 A_K - 2\alpha A_K\right) - 4\alpha A_K$$

$$= S_{K+1}$$

with

$$S_{K+1} = 2 J_K - S_K - 4\alpha A_K.$$

Thus for the iteration one needs to retain only S_K and A_K from previous iteration and evaluate J_K after each iteration. A discussion of the properties and stability of this scheme will be given in another paper.

b)   Initialization of Particles

In the numerical experiments the macroparticles representing the protons are loaded to satisfy the equilibrium state described by the distribution function

$$f(H - \omega P_\theta, v_z) =$$

$$\lambda_0 \delta (H - \omega P_\theta - K) \ \theta[(v_z + \Delta v_z)(\Delta v_z - v_z)],$$

where H is the hamiltonia perpendicular to the external magnetic field, λ_0, ω and K are constants, P_θ is the canonical angular momentum and

$$\theta(x) = \begin{cases} 1, & x \geq 0 \\ 0, & x < 0. \end{cases}$$

The ion layer that is described by the distribution function
of Eq. (1) is in a rigid rotor equilibrium[13] with zero average
axial velocity and with a total axial velocity spread of $2 \Delta v_z$.

The evolution of the system is determined by following
the trajectories of 6000 to 24000 macroparticles in the exter-
nally applied magnetic and self-consistent magnetic fields
produced by the particles.

The distribution function of Eq. (1) requires that at
$t = 0$ the following constraints be satisfied:

$$< v_z > = \int d^3 r \, v_z \, f = 0 \tag{2}$$

$$< v_R > = \int d^3 r \, v_R \, f = 0 \tag{3}$$

and

$$< v_\theta (r) > = \int dz r v_\theta f = \omega r. \tag{4}$$

To insure that the conditions of Eqs. (2) - (4) are satisfied,
an octet of particles is loaded at each initializing position.
A random value of v_z is selected between 0 and Δv_z. Four of
the particles are given the velocity Δv_z and the other four
are given $- \Delta v_z$. The radial velocity is assigned in a similar
manner. The final component v_θ is given by adding and sub-
tracting a random velocity from ωr. The result is that each
of the eight particles in an octet is given in a different
position in velocity space. The positions of the particles
in the octet are then randomized within a specified radial region.

8

c) Diagnostics

One of the main diagnostics used to determine whether the system is stable or unstable is the evaluation of the equipartion of the magnetic energy of the system in the axial Fourier modes. Using the relations $\nabla \times \vec{A} = \vec{B}$ and $\vec{\nabla}^2 A = - \mu_0 \vec{J}$ in the expression for the magnetic energy of the system

$$\varepsilon = \int d^3 r \, \frac{\mu_0 B^2}{2}$$

and after integrating by parts, we find

$$\varepsilon = - \mu_0 \int d^3 r \, \vec{J} \cdot \vec{A} = - \pi \mu_0 \int r J_\theta A_\theta \, dr dz. \tag{5}$$

Substituting in Eq. (5) the Fourier expansion of $\vec{J}$ and $\vec{A}$, it is obtained

$$\varepsilon = -\pi \mu_0 \int dr \, r \sum_{k=0}^{N-1} j_k \sum_{\ell=0}^{N-1} a_\ell \sum_{m=0}^{N-1} e^{\frac{2\pi i (k+\ell) m}{N}} \Delta_z, \tag{6}$$

where N is the number of axial cells and the integral over z has been reduced to a sum over m. Using the identity

$$\sum_{m=0}^{N-1} e^{\frac{2\pi i L m}{N}} = N, \quad \text{for } L = 0 \text{ and } L = N$$
$$= 0, \text{ otherwise}$$

9

Eq. (6) becomes

$$\varepsilon = -\pi\mu_0 \int dr \; r \sum_{k=0}^{N-1} j_k \; a_{N-k}. \tag{7}$$

Because both J and A are real quantities

$$a_{N-k} = a_k^*,$$

and

$$j_{N-k} = j_k^*.$$

Substituting these two relations into Eq. (7), the magnetic energy takes the following form

$$\varepsilon = -\pi\mu_0 \int \left(j_0 a_0 + 2\sum_{k=1}^{N/2} j_k a_k^* \right) rdr,$$

or

$$\varepsilon = e_0 + \sum_{k=1}^{N/2} e_k,$$

where

$$e_k = -2\pi\mu_0 \Delta z \int (j_k \; a_k^*) \; rdr,$$

and

$$e_0 = -\pi\mu_0 \Delta z \int j_0 \, a_0^* \, rdr.$$

The quantities e_k may be identified as the magnetic energy associated with the k - th eigenmode of the system. Initially most of the magnetic energy in a layer will be in e_0 because initially J_θ and A_θ do not vary *in z. In unstable systems* the dominate non-zero mode corresponds to the number of rings that the layer has formed.

III. THEORETICAL PREDICTIONS

a) Stabilization with an Axial Velocity Spread

The tearing mode stability properties of a strong ion layer immersed in a background plasma have been studied recently by Uhm and Davidson.[7] Using a hybrid model, in which the thin ion layer is treated kinetically and the background plasma as a fluid, they have investigated perturbations with frequencies $|\omega| \leq \hat{\omega}_{ci}$, where $\hat{\omega}_{ci}$ is the ion cyclotron frequency at the outer edge of the layer. When the radial thickness 2a of the layer is much smaller than its mean radius R_0, they have shown that perturbations are stabilized when the axial velocity spread Δv_z of the ions in the rotating layer exceeds a critical velocity spread given by

$$\frac{\Delta v_{crit}^2}{(R_0 \hat{\omega}_{ci})^2} = \left[1 - (R_0/R_c)^2 \right] \frac{\nu}{(1+\nu)^2} \left(1 + \frac{\nu a}{3R_0} \right), \quad (8)$$

11

where R_c is the radius of conducting wall surrounding the layer and ν is the Budker parameter.

An important feature of Eq. (8) is that the critical axial velocity spread required for stabilization is independent of the background plasma and therefore should be valid even when the plasma density goes to zero as in the computer simulation.

b) Wall Stabilization

A conducting outer wall plays an important role in the tearing mode. The expression for Δv_{crit} shows that when $R_o = R_c$ the system is stable to tearing instability. The behavior of a system in which all parameters except the wall radius are held constant is much more complex than equation (8) would indicate at first sight. This is due to $\hat{\omega}_{ci}$ being a function of the wall radius. Specifically

$$\hat{\omega}_{ci} = - (\nu+1) \omega_{co} \left[\nu (2 x^2 - 1) - 1 \right]^{-1} , \qquad (9)$$

where ω_{co} is the ion cyclotron frequency in the external magnetic field B_o and $x = R_o/R_c$.

After substitution of Eq. (9) into Eq. (8) we obtain

$$\Delta v^2_{crit} = V^2 F (x) \qquad (10)$$

12

where

$$F(x) = \frac{(1-x^2)\nu}{[\nu(2x^2-1)-1]^2} ,$$

and

$$V^2 = \left(1 + \frac{\nu a}{3R_O}\right) R_O^2 \omega_{CO}^2 .$$

V is a function of ν but is independent of the wall radius. In the limit of a thin beam, i.e., for $a \to 0$, V is independent of ν. F(x) is a complicated function containing a singularity. Figure 1 shows the dependence of F(x) on R_O/R_C for $\nu = 0.3$, 0.8 and 2.0. Because of the singularity F(x) is artifically suppressed in the plot.

$R_O/R_C = 0$ corresponds to no wall or the limit as the wall is removed to infinity. The other extreme $R_O/R_C = 1$ corresponds to a very thin beam against the conducting wall. The lower the value of F(x) the less the thermal spread required to obtain a stable layer. As shown in Fig. 1 the function F(x) is characterized by three distinct regions. For $\nu < 1/3$, F(x) is monotonically decreasing as R_O/R_C increases. Thus, if a system is stable with no conducting wall (i.e., $R_O/R_C = 0$) it is stable for all values of R_O/R_C. For $1/3 < \nu < 1$, F has a maximum and therefore the system requires a greater axial velocity spread to be stabilized

13

as the conducting wall moves from far away closer to the layer. For values of (R_O/R_c) greater than that corresponding to the peak of $F(x)$, the equilibrium becomes more stable. For $\nu > 1$, the function $F(x)$ has a singularity at $(R_O/R_c)_{sin} = (1 + \nu)/2\nu^{\frac{1}{2}}$. The conducting wall has a destabilizing effect on the layer when its radius is such that the condition $R_O/R_c < (R_O/R_c)_{sin}$ is satisfied. In contrast, when the wall is located very close to the outer surface of the layer, i.e., where $R_O/R_c > (R_O/R_c)_{sin}$ the stability of the system is improved. Note that at the singularity equilibrium exist only when the external magnetic field is equal to zero.

IV. RESULTS OF SIMULATIONS

Simulations using 6 to 24 thousand macro-particles show excellent agreement with the predictions of Eq. (8) even when the inequality $a << R_O$ is not satisfied, provided that R_O is set equal to $\left[(R_1^2 + R_1^2)/2\right]^{\frac{1}{2}}$, where R_1 is the inner and R_2 is the outer radii of the layer.

The noise level of the system varies as (number of particles)$^{-\frac{1}{2}}$. Since the number of particles in the simulation is limited, even a stable system for which the linear theory would predict no growth, the axial components of the Fourier spectrum will be non-zero with the equilibrium fluctuation level determined by the number of particles used in the simulation.

Although some degree of randomness is provided by the initialization process, it is well below the final thermal levels found in stable equilibria. For this reason each plot of the energy in the eigenmodes is characterized by an initially fast rising segment which is terminated by reaching the thermal level, usually after one angular rotation period.

Figure 2 shows the noise levels vs. the normalized time $t\omega_R = t\omega_{ci} (\nu+1)^{-1}$ from two simulations with 6000 and 24000 macro-particles stabilized by axial temperature. The two simulations are identical except for the number of particles. The noise drops by about a factor of two when four times as many particles are used.

Figure 3 shows details from the simulation of 6000 macro-particles. In this run the Budker parameter is 2, the inner and outer radii of the layer are 20 and 26 centimeters respectively, the wall radius is 32 centimeters, the applied magnetic field is 10 kilogauss and the thermal spread is 1.2 times greater than the critical value. The periodic temporal variation of the individual axial components corresponds roughly to the time required for a particle with average axial velocity to move a wavelength.

If the thermal spread Δv is less than Δv_{crit}, the modes grow with time. A comparison of the growth rates of individual modes with those predicted by linear theory[14] for $n_p = 0$ shows a discrepancy of about a factor of two, with the code

consistently giving lower growth rates. Figure 4 shows the time development of an unstable system. All the parameters are identical to the stable case except that the initial axial thermal spread is a quarter of the value required for stability i.e., $\Delta v_z = 0.25 \, \Delta v_{crit}$. The measurement of growth rates is complicated by the existence of the ambient noise. The growth rates are compared to the theory when the long wavelength axial modes have established a measurable growth rate.

As the layer tears the axial distribution function changes from the initially square configuration to a more Maxwellian shape. Figure 5 shows the rather dramatic broadening that has occurred by the time the growth rates are measured. The broader profile probably accounts for the discrepancy between our measurements and the theory. The broadening is indicative of the bulk heating of the layer. The unstable spectrum initially grows for short wavelengths and as the heating stabilizes these modes the evolution continues towards longer wavelengths.

The correlation between the energy in the dominant eigenmode and the number of rings that a layer has broken into is illustrated in Fig. 6. As shown in Fig. 4 the system is dominated at $t = 6 \, \omega_R^{-1}$ by the second eigenmode. As expected the system has formed two well defined particle rings at this time. In the final stages of development the layer is dominated

16

by the one mode and consists of a single ring. An examination
of the axial velocity distribution reveals that in this fixed
state that the particles have a spread greater than the criti-
cal spread required for stabilization.

To verify the possible destabilizing influence of a
conducting wall, simulations of two nearly identical but care-
fully selected systems were made. The only external difference
between the two systems was the radius of the conducting outer
wall. The layer extended from 8.8cm to 16.8cm, was immersed
in an external axial magnetic field of 10 kilogauss and had a
Budker parameter of 2. With the outer wall at 32cm an axial
thermal spread was selected to give stability. This same
thermal spread, however, was not sufficient to stabilize the
layer if the wall radius was reduced to 21cm.

The two cases described correspond to $R_O/R_C = 0.4$ and
0.6 for a Budker parameter greater than one as seen in Fig. 1.
A time history of the energy in the axial structure of the two
systems is shown in Fig. 7. For the case $R_O/R_C = 0.4$ (the
more distant wall) the layer developes to the thermal level
and does not grow. For $R_O/R_C = 0.6$ (the close wall) the layer
exhibits growth in the axial modes well above the thermal level
and tears.

V. SUMMARY AND CONCLUSIONS

These computer simulation experiments have verified the
predictions of Uhm and Davidson's theory about the critical

axial velocity spread required to stabilize the tearing mode in an infinitely long ion layer. Although the theory has developed under the assumption that the thickness of the layer is much smaller than its average radius, the results of the simulation have shown that the predictions of the theory are even valid when a $<< R_O$, provided that R_O is set equal to the geometric mean radius of the layer.

The most important conclusion of the present work is on the effect a conducting tube surrounding the layer has on its stability. For a very long time, it has been commonly accepted that a conducting waveguide improves the tearing mode stability properties of the layer. However, our results show that when $\nu > 1/3$, a conducting wall may have destabilizing influence on the layer.
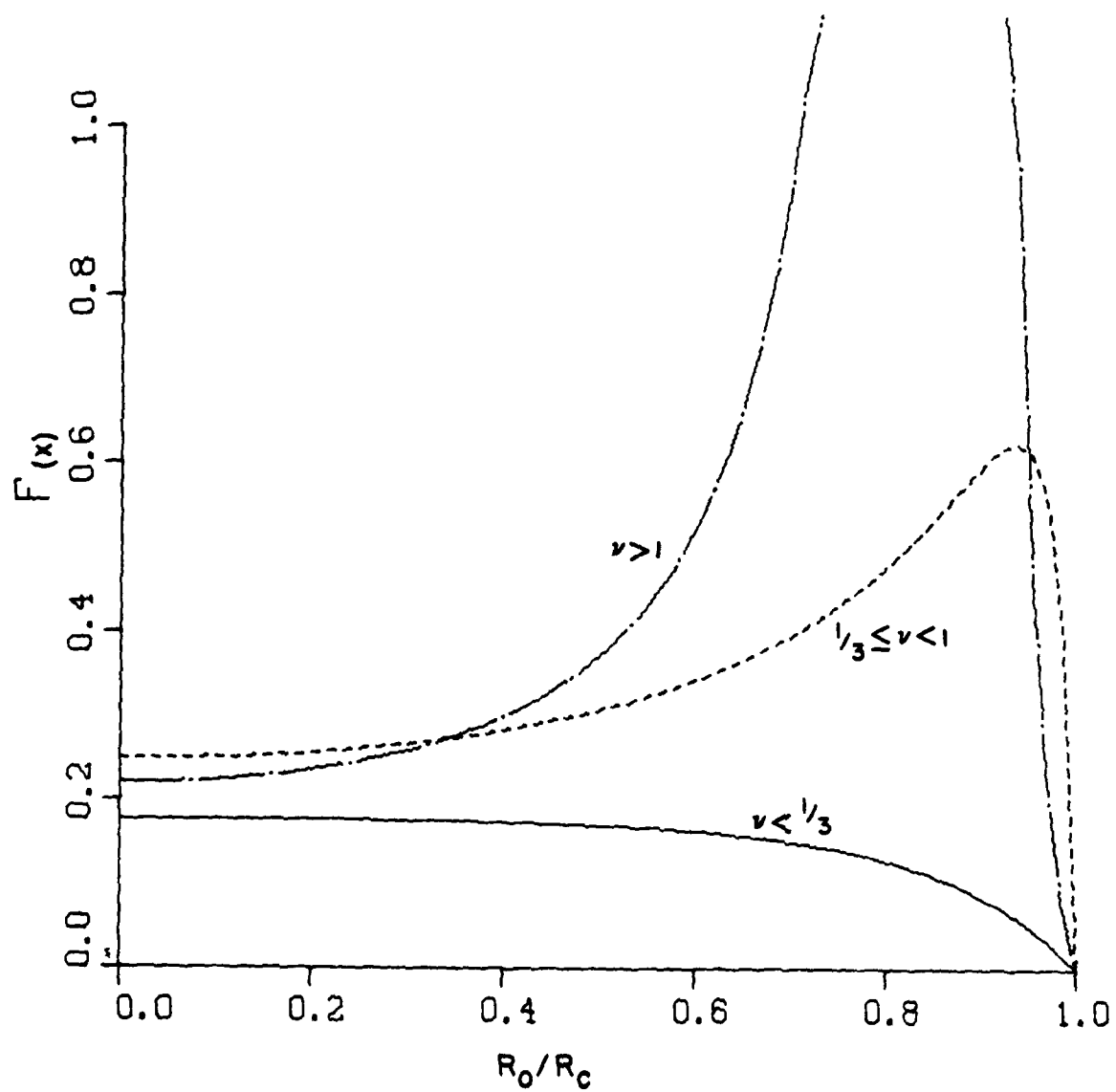
Fig. 1 - Dependence of critical thermal spread on wall radius. Solid line is for a Budker parameter less than 1/3. Dashed line is for a Budker parameter greater than 1/3 and less than 1. Chain-dot is for a Budker parameter greater than 1.
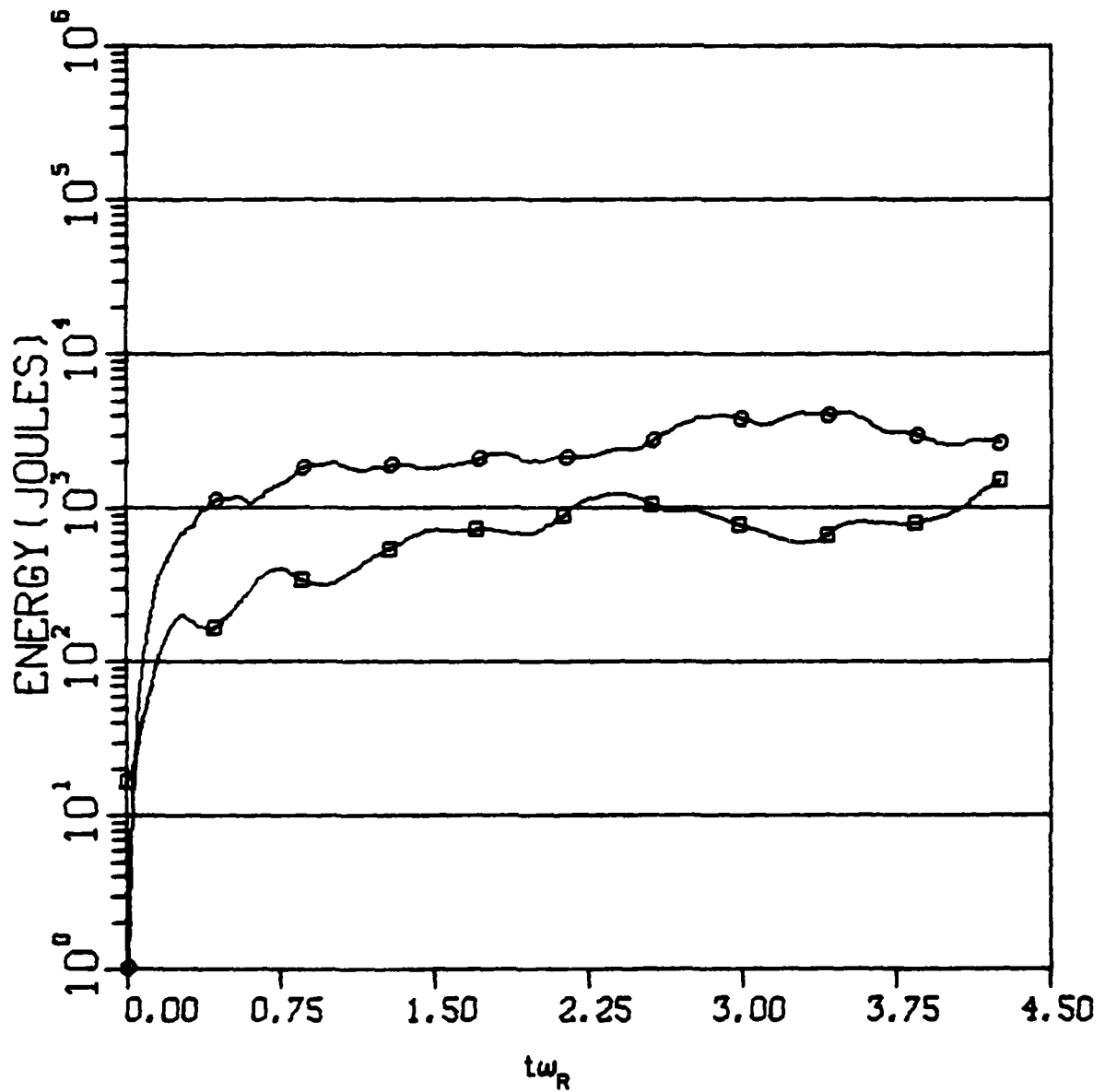
Fig. 2 - Noise levels in identical systems with different numbers of macro-particles. Upper curve corresponds to about 6,000 and lower curve corresponds to 24,000 macro-particles.

20
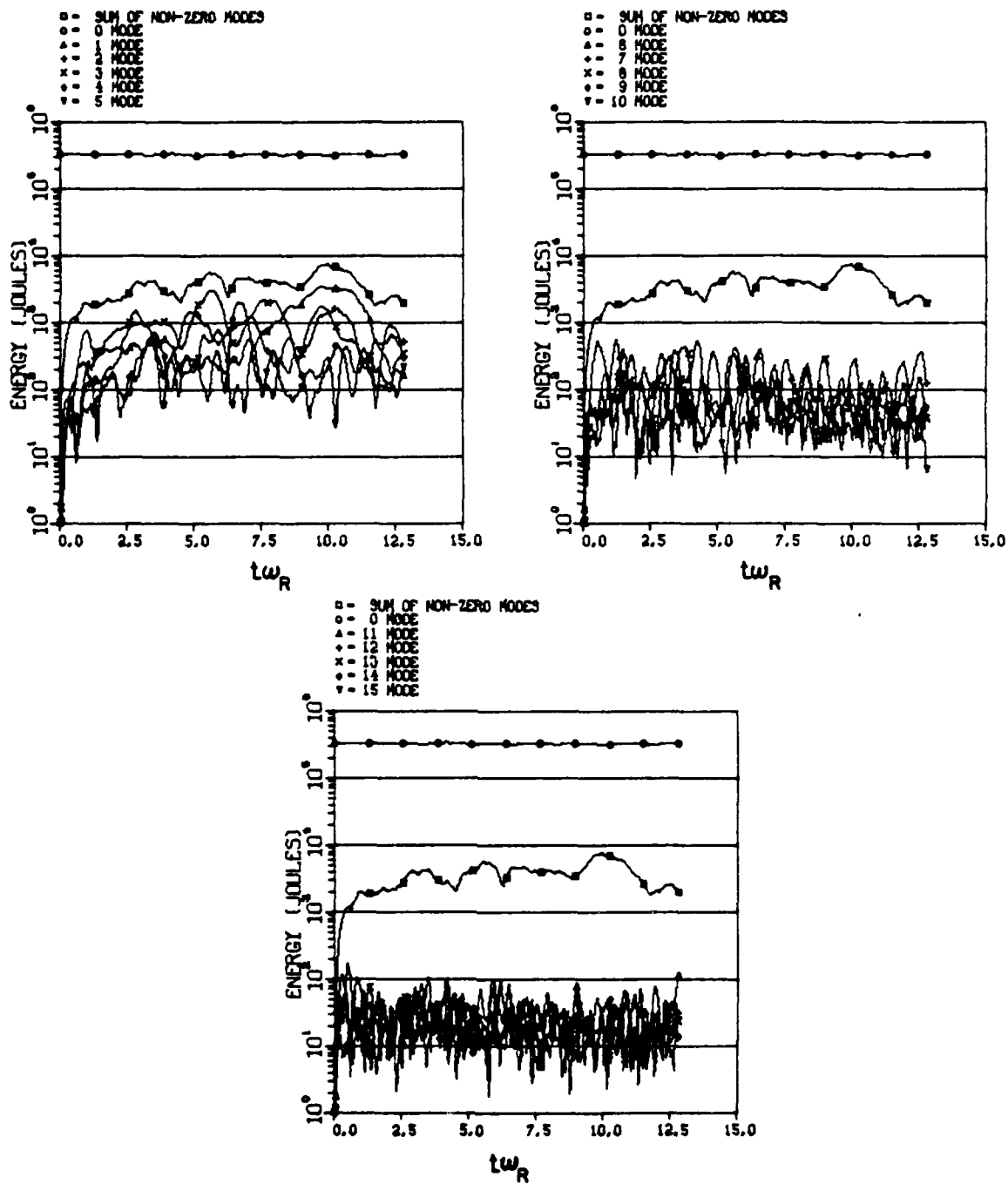
Fig. 3 - Energy in axial Fourier spectrum vs time in a system stabilized by axial thermal spread. The parameters are given in the text.

21
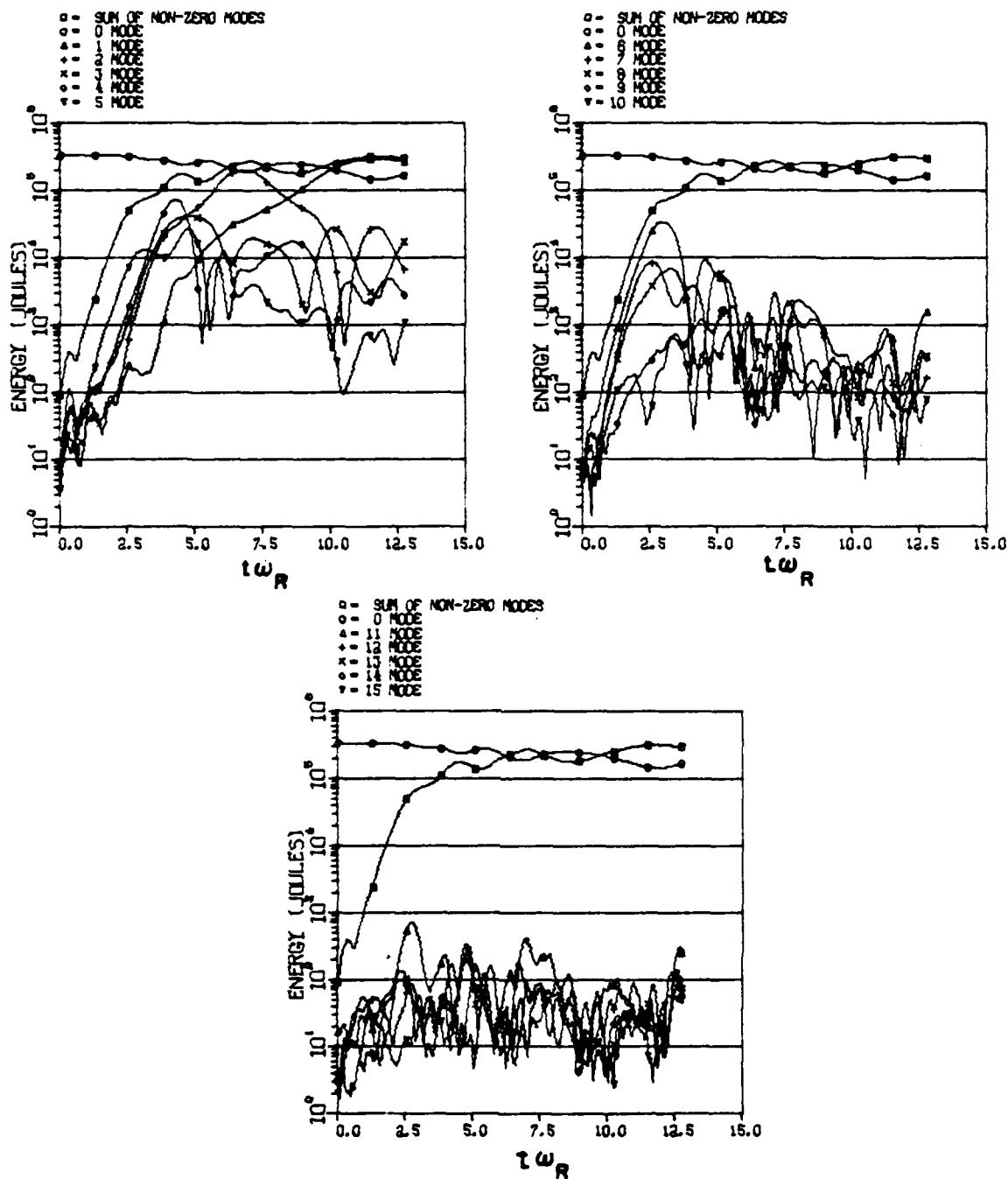
Fig. 4 - Time development of an unstable system: $\Delta v_z = 0.25 \, \Delta v_{crit}$.
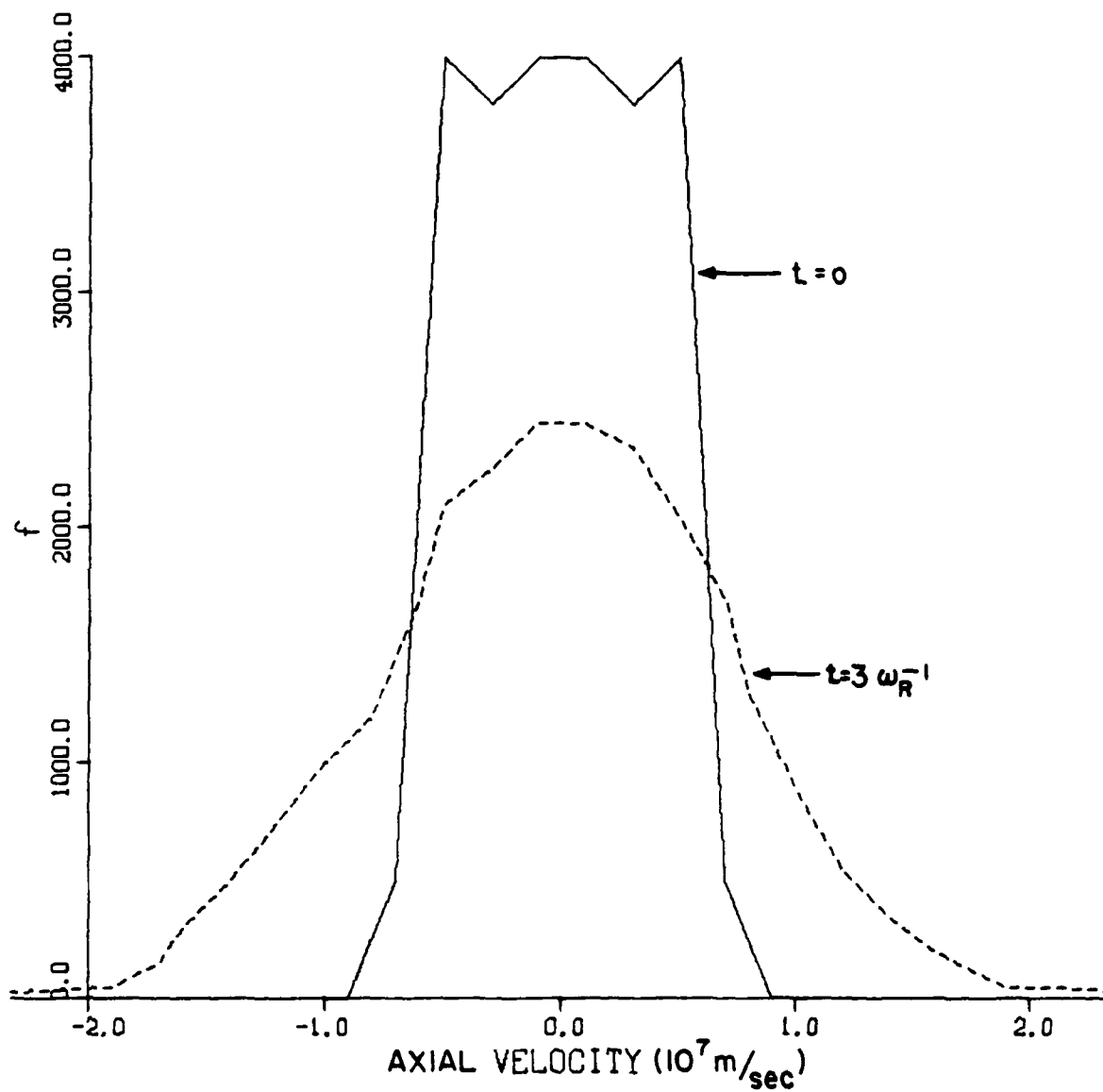
Fig. 5 - Axial distribution function of an unstable system at $t = 0$ and $3\,\omega_R^{-1}$ sec.

23
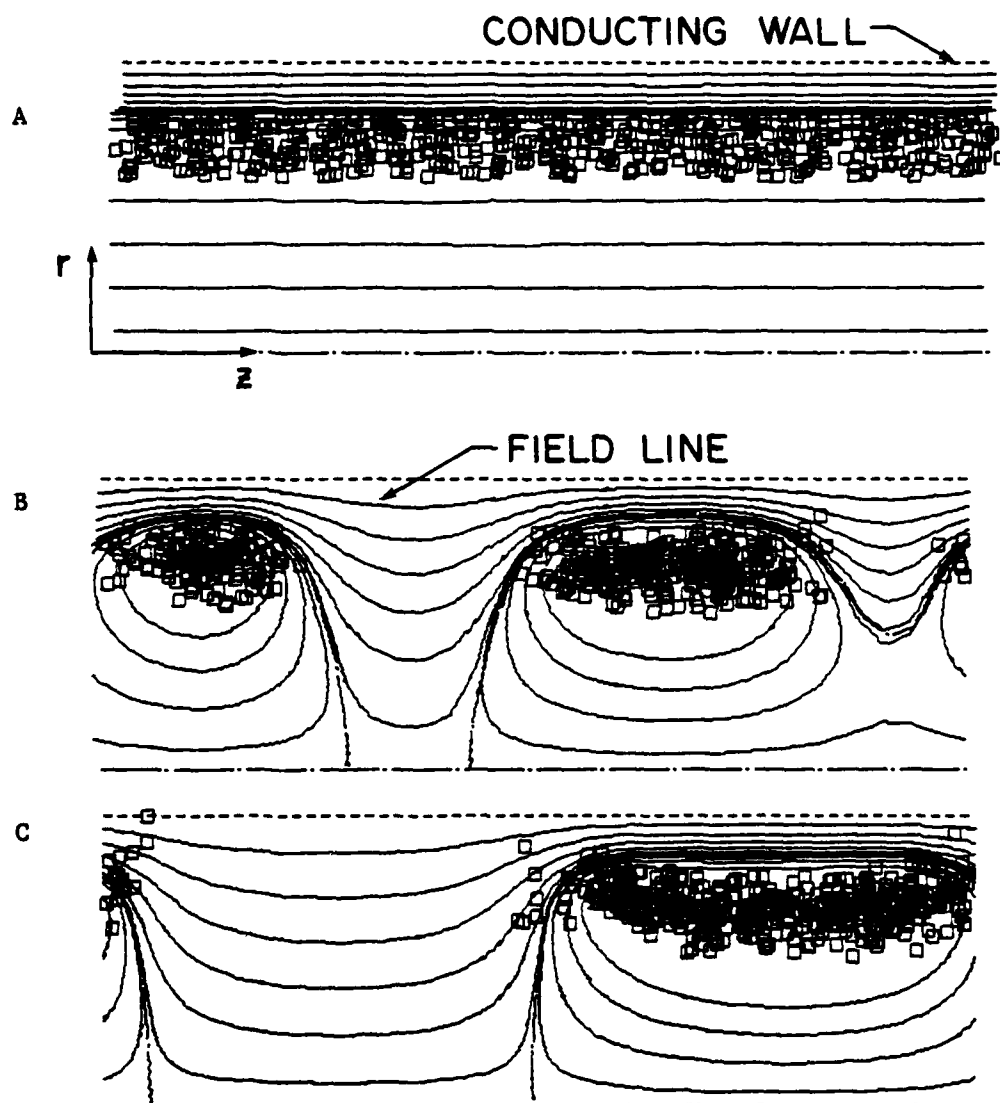
Fig. 6 - Sample particles in unstable system at a) t = 0,
b) $t = 6\omega_R^{-1}$ and c) $t = 12\omega_R^{-1}$.
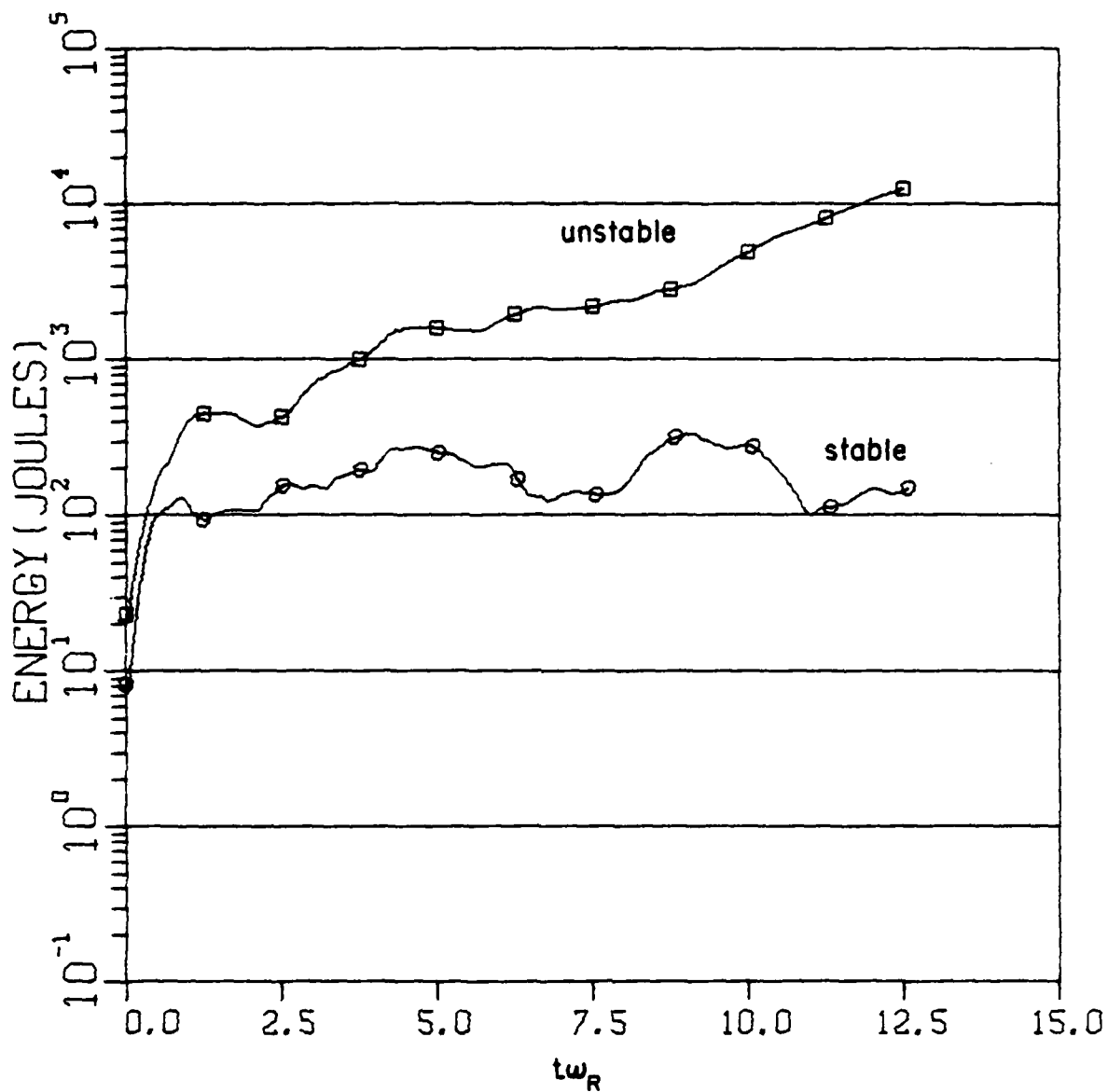
Fig. 7 - Total energy in axial modes of two nearby identical systems. System is destabilized when surrounding conducting wall is moved closer to the outer edge of the layer.

REFERENCES

1. See for example: J. Golden, C. A. Kapetanakos, J. A. Pasour and R. A. Mahaffey, Intense Pulsed Ion Beams, NRL report No. 4162 (1980).

2. K. R. Chu and C. A. Kapetanakos, Nuclear Fusion 15, 947 (1975).

3. See for example: R. F. Post, 4th Intern. Conf. on Driven Magnetic Fusion Reactors, Erice, Italy, Sept. 18-26, 1978.

4. W. C. Condit, G. A. Carlson, R. S. Devoto, J. N. Doggett, W. S. Neef, J. D. Hanson, LLL Report UCRL-52170 (1976).

5. R. N. Sudan and M. N. Rosenbluth, Phys. Rev. Lett. 36, 972 (1976).

6. R. V. Lovelace, Phys. Rev. Lett. 35, 162 (1975).

7. H. S. Uhm and R. C. Davidson, M.I.T., Plasma Fusion Center Report

8. J. M. Finn and R. N. Sudan, Phys. Rev. Lett. 41, 695 (1978).

9. K. D. Marx, Phys. Fluids 11, 357 (1968).

10. H. S. Uhm and R. C. Davidson, M.I.T. Plasma Fusion Center Report JA-79-2 (1979).

11. T. K. Fowler, Phys. Fluids 15, 2075 (1972).

12. S. J. Marsh, A. T. Drobot, J. Golden and C. A. Kapetanakos, Phys. Fluids 21, 1045 (1978); also Phys. Rev. Lett. 39, 705 (1977).

13. C. A. Kapetanakos, J. Golden and K. R. Chu, Plasma Phys. 19, 387 (1977).

14. Uhm, private communication.

Prof. George Bekefi
Bldg. 36-213
Mass. Inst. of Technology
77 Massachusetts Ave.
Cambridge, Mass. 02139

Dr. Jim Benford
Physics International Co.
2700 Merced St.
San Leandro, CA 94577

Dr. Kenneth D. Bergeron
Plasma Theory Div. - 5241
Sandia Laboratories
Albuquerque, Nex Mexico, 87115

Dr. V. M. Birtritsky
Lenina 2a
Research Institute of Nuclear Physics
Tomsk, USSR

Dr. A. E. Blaugrund
Weizman Institute of Science
Rehovot, Israel

Dr. R. Briggs
Lawrence Livermore Laboratory
P. O. Box 808
Livermore, CA 94550

Dr. Blake E. Cherrington
Dept. of Electrical Engineering
University of Illinois
Urbana, IL 61801

Prof. G. Contopoulos
Dept. of Astronomy
University of Athens
Athens, Greece

Prof. R. Davidson
Plasma Fusion Center
Massachusetts Inst. of Technology
Cambridge, MA 02139

Dr. H. J. Doucet, Director
Laboratoire de Physique
  des Milieux Ionises
Ecole Polytechnique
Plateau de Palaiseau
91120 Palaiseau, France

Dr. W. Dove
Dept. of Energy
Washington, DC 20545

Dr. H. Dreicer
Director
Plasma Physics Division
Los Alamos Scientific Lab.
Los Alamos, N. M.   87544

Prof. W. E. Drummond
Austin Research Associates
1901 Rutland Drive
Austin, TX 78758

Dr. A. Fisher
Physics Dept.
Univ. of California
Irvine, Cal.   92664

Prof. H. H. Fleischmann
Lab. for Plasma Studies and
  School of Applied and Engr. Physics
Cornell University
Ithaca, New York 14850

Dr. T. K. Fowler
Assoc. Director for Magnetic
  Fusion Energy
Lawrence Livermore Laboratory
P. O. Box 808
Livermore, CA 94550

Prof. D. Hammer
Lab. of Plasma Studies
Cornell University
Ithaca, New York, 14850

Prof. R. Helleman
Georgia Institute of Technology
Atlanta, Georgia, 30332

Dr. S. Humphries
Sandia Laboratories
Albuquerque, New Mexico, 87115

Prof. H. Ishizuka
Dept. of Physics
Univ. of Tsukuba
Ibaraki, 300-31, Japan

Prof. K. Karoumbalos
Dept. of Physics
University of Athens
Athens, Greece

Dr. Takaya Kawabe
Institute of Plasma Physics
Nagoya University
Nagoya 464
Japan

Dr. J. D. Kilkenny
Dept. of Physics
Imperial College
Prince Consort Road
England

Dr. Peter Korn
Maxwell Labs.
San Diego, CA 92125

Dr. D. Lebedev
Academy of Sciences of USSR
P. N. Lebedev Physical Institute
Moscow, Leninsky Prospect, 53 USSR

Prof. R. V. Lovelace
School of Applied and Eng. Physics
Cornell University
Ithaca, New York, 14853

Dr. S. C. Luckhardt
Plasma Fusion Center
Mass. Inst. of Technology
Cambridge, MA 02139

Prof. T. C. Marshall
School of Eng. and Appl. Science
Plasma Laboratory
S. W. Mudd Bldg.
Columbia Univ.
New York, NY 10027

Dr. D. A. McArthur
Sandia Lab.
Albuquerque, New Mexico 87115

Prof. J. E. McCune
Dept. of Aero. and Astro.
Mass. Institute of Tech.
77 Massachusetts Ave.
Cambridge, Mass. 02139

Prof. G. H. Miley
Chairman
Nuclear Eng. Program
214 Nuclear Eng. Lab.
Urbana, IL 61801

Prof. A. Mohri
Institute of Plasma Physics
Nagoya University
Nagoya, Japan

Dr. Ralph Moir
 L-386
Lawrence Livermore Lab.
P. O. Box 808
Livermore, CA 94550

Prof. J. Nation
Lab. of Plasma Studies
Cornell University
Ithaca, NY 14850

Dr. Joan Ogden
Princeton Plasma Lab.
Princeton, New Jersey

Dr. C. L. Olson
Sandia Lab.
Albuquerque, New Mexico 87115

Dr. I. I. Pervushin
Academy of Sciences of USSR
Radiotechnical Institute
8 Marta Str. 10-12
125083 Moscow A-83, USSR

Dr. R. Post
Lawrence Livermore Laboratory
University of California
P. O. Box 808
Livermore, CA 94550

Dr. D. S. Prono
Lawrence Livermore Laboratory
P. O. Box 808
Livermore, CA 94550

Dr. S. Putnam
Physics Intern. Co.
2700 Merced St.
San Leandro, CA 94577

Prof. N. Reiser
Dept. of Physics and Astronomy
University of Maryland
College Park, MD 20742

Dr. M. E. Rensink
Lawrence Livermore Laboratory
University of California
P. O. Box 808
Livermore, CA 94550

Mr. D. Rej
Lab for Plasma Studies
Cornell University
Ithaca, NY 14853

Dr. J. A. Rome
Oak Ridge National Lab.
Oak Ridge, Tenn. 37850

Prof. Norman Rostoker
Dept. of Physics
University of California
Irvine, CA 92664

Dr. L. I. Rudakov
I. V. Kurchatov Institute of Atomic
Moscow, USSR   Energy

Prof. D. D. Ryutov
Sibirian Branch of Academy of Science
   of U. S. S. R.
Institute of Nuclear Physics
Navosibirsk, USSR

Prof. Hans Schamel
463 Bochum -
RUHR-Universität W. Germany

Prof. George Schmidt
Physics Dept.
Stevens Institute of Technology
Hoboken, New Jersey 07030

Prof. P. Seraphim
Electrical Eng. Dept.
National Technical Univ. of Athens
Athens, Greece

Prof. R. Sudan
Lab. of Plasma Studies
Cornell University
Ithaca, New York 14850

Prof. A. W. Trivelpiece
Science Applications, Inc.
San Diego, CA 92123

Dr. S. S. Tserevitinov
Kurchatov's Institute of Atomic Energy
Moscow, USSR

Prof. R. Uzan
Laboratoire D'emission Electronique
Faculte des Sciences
43, Bd du 11 Novembre 1918
69 - Villeurbanne, France

E. S. Weibel
c/o Center do Recharches
   en Physique des Plasmas
Ecole Polytechnique Federale
   de Lausanne
Avenue des Bains 21
CH-1007, Lausanne, Switzerland

Prof. C. B. Wharton
Occidental Research Corp.
2100 SE Main Street
Irvine, CA 92713

Dr. Gerold Yonas
Sandia Lab.
Albuquerque, NM 87115

Prof. A. Bers
Dept. of Electrical Engr.
Mass. Inst. Of Technology
77 Massachusetts Ave.   -
Cambridge, Mass. 02159

Dr. Charles C. Damm
Lawrence Livermore Laboratory
P. O. Box 808
Livermore, CA 94550

Dr. Chip Smith Jr.
Pacific Gas and Electric Co.
77 Beale Street
San Francisco, CA 94106

Dr. G. P. Gupta
Scientific Officer
Bhabha Atomic Research Centre
(MHD Generation Project)
Bombay, India 400085

Dr. A. N. Didenko
Inst. of Nuclear Physics
Tomsk, USSR

Dr. A. C. Kolb
Maxwell Lab., Inc.
San Diego, CA 92123

Dr. J. Dawson
Univ. Of California at
   Los Angeles
Dept. of Physics
Los Angeles, CA 90024

Dr. R. Linford
Los Alamos Scientific Lab.
P.O. Box 1663
Los Alamos, NM 87545

Dr. C.S. Liu
Dept. of Physics
University of Maryland
College Park, MD 20742

Dr. J. McNally, Jr.
Oak Ridge National Lab.
P.O. Box Y
Oak Ridge, TN 37830

Dr. W. R. Ellis
Chief Magnetic Mirror Systems
Office of Fusion Energy
Dept. of Energy
Washington, D.C. 20545

Dr. A. Bromborsky
Harry Diamond Lab.
2800 Powder Mill Rd.
Adelphi, MD 20783

Dr. V.P. Sarantsev
Jt. Institute for Nuclear Res.
Head Post Office P.B. 79, Moscow
Dubna, USSR

Dr. B. Godfrey
Mission Res. Corp.
1400 San Mateo Blvd. S.E.
Suite A
Albuquerque, NM 87108

Prof. C. Striffler
Dept. of E.E.
Univ. of Maryland
College Park, MD 20742

Dr. R.J. Faehl
Los Alamos Scientific Lab.
Los Alamos, NM 87544

Dr. W. Condit
Div. Appl. Plasma Physics
U.S. Dept. of Energy
Washington, D.C. 20545

Dr. J.M. Buzzi
Ecole Polytechnique
Plateau de Palaiseau
91120 Palaiseau, France

Dr. A. Miyahara
Institute of Plasma Physics
Nagoya Univ.
Nagoya 464
Japan

Dr. Shigeo Kawata
Tokyo Inst. of Technology
Tokyo, Japan

Dr. D.A. Johnson
Sandia Nat'l Lab.
Albuquerque, NM 87115

Prof. F. Chen
Dept. of E.E.
Unif. of Calif. at Los Angeles
Los Angeles, Calif. 90024

Mr. J.E. Maenchen
Physics International Co.
2700 Merced St.
San Leandro, CA 94577

Dr. Z.G.T. Guiragossian
TRW Sys. and Energy RI/1070
Advanced Technology Lab.
1 Space Park
Redondo Beach, CA 90278

Dr. S. Graybill
Harry Diamond Lab.
2800 Powder Mill Rd.
Adelphi, MD 20783

Dr. J. Sazama
Naval Surface Weapons Center
Code 431
White Oak, Silver Spring, MD 20910

Dr. J.U. Guillory
Jaycor
20550 Whiting St.
Suite 500
Alexandria, VA 22304

Dr. A. Sternlieb
Lawrence Berkely Lab.
Berkeley, CA 94720

Dr. M. Masuzaki
Inst. of Plasma Physics
Nagoya University
Nagoya, Japan

Dr. D. Straw
AFWL
Kirtland AFB, NM 87117

Dr. H. Uhm
Naval Surface Weapons Center
White Oak, Silver Spring, MD 20910

Dr. J.G. Eden
Dept. of Electrical Engineering
Univ. of Illinois
155 EEB
Urbana, Ill. 61801

Prof. W. Doggett
NC State Univ.
P.O. Box 5342
Raleigh, NC 27650

Prof. B. Dangor
Dept. of Physics
Imperial College of Science and
London S.W.7 England Technology

Dr. Venkat Ramani
554 Exp'l Plasma Physics
Phys. Res. Lab.
Navrangpura Ahmedabad -380-009
India

Dr. C.A. Patou
Ctr. D'Etudes Valduc
B.P. 14
21120 Is Sur Tillie, France

Dr. A. Kolomensky
Lebedeu Physical Institute
Moskow, USSR

Dr. Jen-Chang Chou
Institute of Nuclear Energy Research
P.O. Box 3
Lung-Tan, Taiwan

Dr. M. Caponi
TRW Advance Tech. Lab.
1 Space Park
Redondo Beach, CA 90278

Dr. P.J. Castleberry
Defense Intelligence Agency
Attn. DT-IA
Washington, D.C. 20301

Dr. W.N. Destler
Dept. of Electrical Engineering
Univ. of Maryland
College Park, MD 20742

Dr. C.E. Hollandsworth
Ballistic Research Lab.
DRDAB - BLB
Aberdean Proving Ground, MD 21005

Dr. M. Nahemow
Westinghouse Electric Corp.
1310 Beutah Rd.
Pittsburgh, PA 15235

Dr. W.G. Applegate
CIA
Washington, D.C 20505

Dr. J. Bayless
DARPA attn: DEO
1400 Wilson Blvd.
Arlington, VA 22209

Dr. J. Hyman
Hughes Research Lab.
3011 Malibu Cyn Rd.
Malibu, CA 90265

12 cpys - Defense Documentation Center

20 cpys - Code 2628

25 cpys - Code 4700

75 cpys - Code 4761